Shahid Chamran University of Ahvaz

Iranian Association of Electrical and Electronics Engineers

Journal of Applied Research in Electrical Engineering

E-ISSN: 2783-2864
P-ISSN: 2717-414X
Homepage: https://jaree.scu.ac.ir/

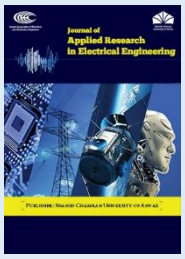

Research Article

Wide Area Robust Controller Design for SSSC to Improve the Oscillations Caused by the Time Delay of Remote Signals

Babak Keshavarz Zahed, and Mohammad Hassan Moradi *

Department of Electrical Engineering, Faculty of Engineering, Bu-Ali Sina University, Hamedan, Iran

** Corresponding Author: mhmoradi@basu.ac.ir*

Abstract: The penetration of double-fed induction generators (DFIG) as renewable energy sources (RES) in power systems leads to fluctuations caused by wind energy. Therefore, based on this challenge, a wide area damping controller (WADC) has been designed to compensate the oscillatory modes by a static synchronous series compensator (SSSC). In addition to the design of WADC for SSSC, a parallel compensator in the form of a supercapacitor energy storage system (SCESS) has been used in the DC link of the wind unit so that DFIG can be used optimally to supply the power system. The design method for compensating time delays in WADC is based on free weight matrices (FWM). First, based on the theory of robust control based on delay-dependent feedback, a set of constraints related to linear matrix inequality (LMI) is formulated. In the following, the free weight matrix (FWM) has been used to solve the delay-dependent time problem. The purpose of applying FWM is to extract the most optimal gain for the controller in the presence of the time delay. The proposed FWM matrix tries to find the most optimal gain in the controller with the help of an iterative algorithm based on the linearization of the conical complement. The simulation results have been implemented in the MATLAB software environment after obtaining the critical modes in the nonlinear time domain on the power system of 16 improved machines. Based on the simulation results, the robustness of the proposed controller under various uncertainties is clearly shown in this paper.

Keywords: Power system, linear matrix inequality, WAMS, SSSC, DFIG, stability.

Article history
Received 28 February 2024; Revised 26 April 2024; Accepted 24 June 2024; Published online 23 October 2024.

How to cite this article
B. Keshavarz Zahed, and M. H. Moradi, "Wide area robust controller design for SSSC to improve the oscillations caused by the time delay of remote signals," *J. Appl. Res. Electr. Eng.*, vol. 3, no. 2, pp. 120-135, 2024.
DOI: 10.22055/jaree.2024.45909.1103

Check for updates

NOMENCLATURE

Synchronous Generator (SG) Variables

E'_{qi} (p.u.)	The field voltage of the SG in the q-axis
E'_{di} *(p.u.)*	The field voltage of the SG in the d-axis
I_{di}	The current of the SG in the d-axis
I_{qi}	The current of the SG in the q-axis
E_{fdi}	The SG excitation field voltage
K_{Ei}	Excitation system controller gain
S_{Ei}	Saturation component of excitation field in SG
V_{Ri}	SG terminal voltage
ω_i	SG rotor angular velocity
ω_s	SG synchronous speed
δ_i	Rotor angle in SG
D_i	Damping coefficient in SG model
L'_{qi}	Transient inductance in the q-axis
L'_{di}	Transient inductance in the d-axis
T_{mi}	Mechanical torque in SG
τ_{ji}	Time constant between generators i and j
X_d	d-axis steady state reactance
X'_d	d-axis transient state reactance

X_q	q-axis steady state reactance
X'_q	q-axis transient state reactance
T'_{doi} (s)	The time constant of the d-axis
T'_{qoi}(s)	The time constant of the q-axis
H(s)	Inertia constant in SG
DFIG Variables	
i_{dsw}	Stator current SG in d-axis
i_{qsw}	Stator current SG in q-axis
i_{drw}	Rotor current SG in d-axis
i_{qrw}	Stator current SG in q-axis
H	Inertia constant in DFIG
R_s	Stator winding resistance
L_{rr}	Rotor internal inductance
L_{mm}	Field self-inductance
L_{ss}	Stator self-inductance
V_{drw}	DFIG rotor voltage in d-axis
V_{qrw}	DFIG rotor voltage in q-axis
R_r	Rotor winding resistance
V_{qsw}	DFIG stator voltage in d-axis
V_{qsw}	DFIG stator voltage in d-axis
ω_s	Synchronous speed of induction generator
ω_r	Rotor speed of induction generator

SCESS-SSSC Variables	
i_{sc}	Storage current
L_S	Circuit inductance SCESS
f_S	SCESS switching frequency
V_{DC}	DC voltage
C_{SC}	SCESS orbital capacity
$V_{C_{SC}}$	Capacitor voltage in SCESS
$R_{P_{SC}}$	Parallel branch resistance in SCESS
v_{ds}	SSSC voltage on d-axis
v_{qs}	SSSC voltage on d-axis
m_c	Modulation index in SSSC inverter
Z_{inv}	Inverter filter impedance in SSSC
V_{dc_sssc}	DC voltage in SSSC
α_{se}	SSSC inverter fire angle
C_{dc}	Capacitance of the dc link in SSSC
i_d	SSSC current in d-axis
i_q	SSSC current in q-axis
R_{dc}	DC link resistance in SSSC

1. INTRODUCTION

1.1. Background and Motivation

One of the most popular RES to produce electrical energy is the use of wind energy. But due to wind speed fluctuations, the use of these units in the power system leads to additional fluctuations. Therefore, controlling fluctuations caused by variable speed wind units is essential and important from the point of view of stability in the power system [1-2]. For this purpose, the presence of energy storage systems (ESS) along with flexible alternating current transmission systems (FACTS) in the power system leads to increased damping of fluctuations and reliable utilization [3-4].

One of the most popular types of variable speed wind turbines is DFIG. The use of these generators is more common than other wind units because of the direct control of active and reactive powers and the type of protection in the way of connecting the converters to each other [5]. In the DFIG structure, a back-to-back two-way converter is used as a grid-side converter (GSC), a rotor-side converter (RSC) and a control loop for the DC link capacitor to connect the two converters [6]. The use of SCESS in the DC link of a DFIG leads to soft start-up and, as a result, reduces fluctuations caused by wind [7].

1.2. Literature Review

In the studies of low frequency oscillations (LFO) of the power system to identify local modes (frequency range 0.9 to 2 Hz) and inter-area (frequency range 0.2 to 0.9 Hz) design of power system stabilizers (PSS) and power oscillation dampers (POD) is considered useful for synchronous generators (SG) and FACTS devices[8]. In the family of FACTS devices, the SSSC compensator is placed in series in the transmission line and controls the power flow in the transmission line [9]. Among the useful methods for SSSC controller design are non-linear robust control in damping local fluctuations and improving transient stability [10], methods based on intelligence for optimal selection of controller parameters in PSS-SSSC coordinated design [11, 12], model predictive control (MPC) and sliding mode control (SMC).

Due to the expansion of the dimensions of power systems, it is not possible to control inter-area fluctuations through the identification of local modes. Therefore, to control the inter-area modes, it is necessary to use the wide area measurement system (WAMS), in which the signals caused by the inter-area modes can be measured and sent by phasor measurement units (PMU) at different points of the power system. [13]. In this type of operation, the feedback signal (containing information about inter-regional modes) is applied to the input of WADC controllers [13]. However, the information resulting from the feedback signal due to the use of telecommunications equipment and sending from a remote area is associated with time delays that must be considered in the design of WADC [14]. In various researches for time delay compensation, methods such as Padé approximation [15], MPC method [16], loop shaping [17], H2/H∞ robust control [18, 19], reinforcement learning method [20], Linear quadratic estimator (LQE) is proposed in [21] and robust controller by solving Lyapunov function (LF) problem [22, 23]. The state estimation method is one of the methods that require high accuracy to determine the characteristics of the power system. Therefore, as the dimensions of the power system increase, extensive measurement is required, which leads to a high order of system states [24, 25].

The hybrid particle swarm optimization method is a simple yet practical method that has been used to optimize WADC controller parameters in the presence of time delays in various researches [26]. Among other optimization methods, we can refer to the reinforcement learning method based on policy gradient using neural networks [27]. However, in this method, because the system model is not available, a very extensive discretization operation is needed to identify it. Analysis of dynamic modes based on an online model is a method introduced in the measurement of WADC signals in [28]. The basis of this method is based on singular value decomposition (SVD). This depends on the accurate low-order model in the dynamics of the power system. Using SVD to reduce the order of power system and design with discrete linear quadratic regulator (LQR) for WADC controller is a method introduced without considering time delay in [28]. Network Predictive Control (NPC) is another online model identification method that is introduced in the WADC design for the rotor side converter (RSC) of a wind farm [29]. One of the important advantages of NPC is considering the physical constraints of the system in the online optimization process. However, in order for the prediction of system outputs to be valid, it is necessary to be very careful in identifying the online model of the plant. In WADC design, it is very important to try to increase the delay margin to compensate for the time delay. Based on this, in [30], the delay margin has been designed for second-order oscillatory modes with respect to fixed delays, square wave and gamma distribution. In this design method, a probability distribution function is used in order to be able to consider the special values of the oscillatory modes in the presence of random delays. However, no method is considered for the distribution of the probability function.

1.3. Research Gap and Contribution

The use of Lyapunov functions is another problem solving method in order to prove stability, which can be effectively useful in WADC design. With the help of the LMI criterion, the stability of the Lyapunov function can be obtained, which can be proved by its negative derivative. The application of LMI in wide area systems is to obtain the gain of controllers in the presence of time delays. In other words, it can be said that through LMI, matrices with large dimensions are solved faster, and therefore the imbalance of the system due to the existence of time delays is avoided [31]. However, the big disadvantage of LMI is its high degree of conservatism, which through the LF; we are looking for solutions that can achieve this degree of conservatism along with the desired stability. Therefore, the design of a suitable LF should include variables that, in addition to maintaining the degree of conservatism of LMI, also have the necessary stability. In [32], Pad approximation is used as delay modeling in LMI for WADC design where only fixed delays are controlled. In [33], the problem of solving time-varying delays based on feedback signals by LMI is investigated. However, additional variables and cross terms are not used in the LF structure. Therefore, the analysis of LMI has been done in a very simple way, so that the long-range delay is easily replaced by its boundaries, and as a result, it is not possible to accurately track it.

In [23], the design of the robust damper controller for the power system is transformed into a general H_∞ problem and solved by the LMI method, but the selection of the optimal weight parameters for the H_∞ controller is difficult. Based on the above studies, in this paper, an improved optimal control method based on the FWM approach is used to design the WADC, which has the ability to effectively compensate for time delays. Therefore, the main purpose of the damping controller in this paper is to be able to damp the inter-area modes through the WADC in the SSSC converter. Based on this, first the remote signals are determined by the visibility and controllability index and then it enters the FWM design process as a $u(t-\tau) = Kx(t-\tau)$ signal. Finally, based on the response obtained from the design method, damping signals can be applied to the SCESS control loop along with time delay compensation.

Briefly, the innovations of this paper are presented under the following comments:

- New FWM design to compensate for the uncertainty caused by continuous and disruptive time delays.
- Adapting the FWM method to the LMI in the form of an optimization problem.
- Combined modeling of energy storage system with RES in large-scale power system.

The written structure of this paper is as described in the second part of the supplementary explanations related to WADC design. This section includes subsections related to FWM modeling, observer-based state feedback. The third part is related to the modified 16-machine power system model, the dynamic equations of the synchronous generator and DFIG along with the block diagram of the controllers. In the fourth part, the simulation results have been analyzed and in the fifth part, the conclusion of the proposed method has been reported.

2. THE WADC DESIGN

The use of small signal analysis is a practical method in obtaining the critical modes of the power system for designing optimal gains in damping controllers. Therefore, when using WAMS, the problem of variable time delay should be considered. For this purpose, in this work, Pade's first-order approximation along with the use of low-pass and high -pass filters have been used to model the time delay. In addition to compensating the time delay, the *K* gain related to the state feedback control matrix has been optimally extracted using FWM. On the other hand, the gain matrix *K* is for state variables, and therefore, these states cannot be easily measured in systems with large dimensions. Therefore, in this work, the state observer $O_b(s)$ has been introduced to observe the state variables based on pole placement, so that a more accurate response can be made from the controller design.

2.1. FWM method

Delay-dependent and delay-independent criteria are two methods in the design of delay controllers. Considering that the delay-dependent measure uses delay size information, but the delay-independent stability measure does not need this information; Therefore, the delay-dependent criterion usually has a lower degree of conservatism than the delay-independent criterion, and it becomes more prominent when the time delays are small. The Lyapunov method is a main method for deriving the delay-dependent criterion, in which the discretized Lyapunov is one of the most efficient methods, but combining this method with the control system is very difficult and complicated. Another method is to transform the

fixed model, one of the most effective and practical of which is the combined method of Park's and Moon's inequalities, whose preliminary model is presented in reference [34, 35]. However, extensive research in this field continues. Therefore, the FWM method is proposed as a new method to solve the stability problem in many delayed systems. In the present work, the degree of conservatism of the controller is reduced compared to the fixed model transformation methods. In the fixed model transformation, when the LF derivative is calculated, the upper bound estimate of Park's and Moon's inequality methods should be used. In contrast, the FWM method does not require bounding techniques for some cross terms. To illustrate this, a common stability problem for a delayed system is considered as follows (1):

$$\begin{cases}\dot{x}(t) = \bar{A}x(t) + \bar{B}x(t_1) + \bar{C}u(t) \\ t_1 = t - \tau\end{cases} \quad (1)$$

In (1), $\bar{A}$, $\bar{B}$, and $\bar{C}$ represent fixed real matrices with suitable dimensions. τ is used to represent the time delay and u(t) is used to introduce the input control signal. In this paper, to introduce the Lyapunov function, we describe (2) [31]:

$$\bar{V}(t, x_t) = x^T(t)\bar{P}x(t) + \int_{t_1}^{t} x^T(s)\bar{Q}x(s)ds + \int_{-\tau}^{0}\int_{t+\theta}^{t} \dot{x}^T(s)\bar{Z}\dot{x}(s)dsd\theta \quad (2)$$

In (2), the first and second parts of LF are considered as potential kinetic energy quantities in mechanical systems, and the third term is used for the derivative. $\bar{P} = \bar{P}^T, \hat{Q} = \bar{Q}^T, \bar{Z} = \bar{Z}^T$ expressions should be determined and then the derivative of the LF should be calculated as (3) [31]:

$$\dot{V}(x_t) = \dot{x}^T(t)\bar{P}x(t) + x^T(t)\bar{P}\dot{x}(t) + x^T(t)\bar{Q}x(t) - x^T(t_1)\bar{Q}x(t_1) + \tau\dot{x}^T(t)\bar{Z}\dot{x}(t) - \int_{t_1}^{t} \dot{x}^T(s)\bar{Z}x(s)ds \quad (3)$$

In order to provide the LMI-based stability criterion, using the conventional stationary model transformation and LF, the right-hand side of (4) is usually added to the $V(t, x_t)$ derivative in (3). Based on this, we will have (4) [31]:

$$0 = 2x^T(t)\bar{P}\bar{B}\left[x(t) - x(t_1) - \int_{t_1}^{t} \dot{x}(s)ds\right] \quad (4)$$

In (4), $\bar{B}$ is the matrix of coefficients and $\bar{P}$ is the Lyapunov matrix.

It is clear that for conventional solutions such as time-constant model transformation, inequalities must be solved to satisfy the $\dot{V}(x_t) < 0$ condition; therefore, determining $\bar{B}$ and $\bar{P}$ matrices is a serious limitation in solving classical methods that cannot be obtained freely. For this purpose, in the proposed method to reduce the degree of conservatism of LMI, the derivative of the LF is used in such a way that the matrices *M* and *N* are placed as auxiliary links in the New Leibniz problem instead of $\bar{B}$ and $\bar{P}$. Therefore, calculating the derivative of (3) is equivalent to adding the right side of (5) to $\dot{V}(x_t) < 0$. Then we can provide some LMI inequalities to satisfy the condition. Based on this, we will have:

$$0 = [x^T(t)\bar{M} + \dot{x}^T(t)\bar{N}]\left[x(t) - x(t_1) - \int_{t_1-\tau}^{t} \dot{x}(s)ds\right] \quad (5)$$

So, as seen in the FWM method, there is no need to choose $\bar{B}$ and $\bar{P}$, and it is enough to optimize $\bar{M}$ and $\bar{N}$ by solving the LMIs, so the FWM method reduces the degree of conservatism of the controller for the time delay system.

2.2. Mathematical Modeling for WADC Design Based on FWM Method

This section has been investigated using the modeling of power system components including synchronous machines, wind turbines and loads in the form of state space. In the analysis of the state space matrix, BESS supplementary signal is used as input and WAMS signals are used as output in the design. Furthermore, when the time delay is used as the transmission delay for the WADC controller input, the linearized system model is expressed as (6):

$$\begin{cases}\dot{x}(t) = \bar{A}x(t) + \bar{B}u(t_1) \\ y(t) = \bar{C}x(t)\end{cases} \quad (6)$$

In (6), vectors $\bar{A}$ and $\bar{B}$, and $\bar{C}$ correspond to the state, input, and output matrices, respectively. The state feedback controller can be expressed as (7):

$$u(t_1) = Kx(t_1) \quad (7)$$

According to (5) for the open loop system and also (6) for the expression of the controller, the closed loop system can be described as (8):

$$\begin{cases}\dot{x}(t) = \bar{A}x(t) + \bar{B}Ku(t_1) \\ y(t) = \bar{C}x(t)\end{cases} \quad (8)$$

The purpose of this section is to provide a delay-dependent stability criterion in the new model to optimally provide the controller gain in the presence of time delay, so that the closed-loop system of (8) remains stable. Therefore, with the definition of Lemma 1, we will have:

Lemma 1 (Schur's complement [36]): According to the definition of Schur's complement, in order to make the matrix $(\bar{S} = \bar{S}^T = \begin{bmatrix}\bar{S}_{11} & \bar{S}_{12} \\ \bar{S}_{21} & \bar{S}_{22}\end{bmatrix}(\bar{S}_{11} \in \overline{\Re}^{r\times r}))$ symmetric, the following three conditions must be met:

1. $\bar{S} < 0$
2. $\bar{S}_{11} < 0, \bar{S}_{22} - \bar{S}_{12}^T\bar{S}_{11}^{-1}\bar{S}_{12} < 0$
3. $\bar{S}_{22} < 0, \bar{S}_{11} - \bar{S}_{12}^T\bar{S}_{22}^{-1}\bar{S}_{12}^T < 0$

Theorem 1: In a certain scalar such as *h*, a feedback controller such as (7) can exist for which the closed loop system (8) remains stable, provided there are $Y = \begin{bmatrix}Y_{11} & Y_{12} \\ Y_{21} & Y_{22}\end{bmatrix} \geq 0, \bar{L} = \bar{L}^T > 0, \bar{Q}_1 = \bar{Q}_1^T > 0, \bar{R} = \bar{R}^T > 0$ and matrices $\bar{M}_1$, $\bar{M}_2$, Also, $\bar{V}$ is used in such a way that matrix inequalities (9) and (10) are satisfied [31]:

$$\bar{\Phi} = \begin{bmatrix}\bar{A}\bar{L} + \bar{L}\bar{A}^T + \bar{M}_1 + \bar{M}_1^T + \bar{Q}_1 + \bar{h}\bar{Y}_{11} & \bar{B}\bar{V} - \bar{M}_1 & \bar{h}\bar{L}\bar{A}^T \\ * & -\bar{M}_2 - \bar{M}_2^T & \bar{h}\bar{V}^T\bar{B}^T \\ * & * & -\bar{h}\bar{R}\end{bmatrix} < 0 \quad (9)$$

$$\bar{\Psi} = \begin{bmatrix} Y_{11} & Y_{12} & \bar{M}_1 \\ * & * & -\bar{M}_2 \\ * & * & \bar{L}\bar{R}^{-1}\bar{L} \end{bmatrix} > 0 \quad (10)$$

where the sign * indicates the symmetry of the matrix and $K = \bar{V}\bar{L}^{-1}$ the gain of the feedback controller.

Proof: According to the Newton-Leibniz formula, we have (11):

$$x(t) - x(t_1) - \int_{t_1}^{t} \dot{x}(s)ds = 0 \quad (11)$$

According to (10), for every matrix with appropriate dimensions $\bar{N}_1$ and $\bar{N}_2$, equation (12) is satisfied:

$$0 = 2(x^T(t)\bar{N}_1 + x^T(t_1)\bar{N}_2) \times \left[x(t) - x(t_1) - \int_{t_1}^{t} \dot{x}(s)ds\right] \quad (12)$$

In the definition of any semi-positive definite matrix such as $Y = \begin{bmatrix} X_{11} & X_{12} \\ X_{12}^T & X_{22} \end{bmatrix} \geq 0$, equation (13) can be satisfied [31]:

$$\bar{h}\bar{\xi}^T(t)X\bar{\xi}(t) - \int_{t_1}^{t} \bar{\xi}^T(t)X\bar{\xi}(t)ds > 0 \quad (13)$$

where $\bar{\xi}(t) = [x^T(t), x^T(t_1)]^T$.

Now, by constructing the candidate LF, we will have equation (14) [31]:

$$V(x_t) = x^T(t)\bar{P}x(t) + \int_{t_1}^{t} x^T(s)\bar{Q}x(s)ds + \int_{-\bar{h}}^{0}\int_{t+\theta}^{t} \dot{x}^T(s)\bar{Z}\dot{x}(s)ds d\theta \quad (14)$$

where $\bar{P} = \bar{P}^T > 0, \bar{Q} = \bar{Q}^T > 0, \bar{Z} = \bar{Z}^T > 0$ should be determined.

Then, by calculating the derivative of $V(x_t)$ in (14) for system (8), we will have (15):

$$\begin{aligned} \dot{V}(x_t) &= \dot{x}^T(t)\bar{P}x(t) + x^T(t)\bar{P}\dot{x}(t) + x^T(t)\bar{Q}x(t) \\ &\quad - x^T(t_1)\bar{Q}x(t_1) + \bar{h}\dot{x}^T(t)\bar{Z}\dot{x}(t) \\ &\quad - \int_{t_1}^{t} \dot{x}^T(s)\bar{Z}\dot{x}(s)ds \\ &= x^T(t)[\bar{P}\bar{A} + \bar{A}^T\bar{P}]x(t) + 2x^T(t)\bar{P}\bar{B}\bar{K}x(t_1) \\ &\quad + x^T\bar{Q}x(t) - x^T(t_1)\bar{Q}x(t_1) \\ &\quad + \bar{h}[\bar{A}x(t) + \bar{B}Kx(t_1)]^T\bar{Z}[\bar{A}x(t) + \bar{B}Kx(t_1)] \\ &\quad - \int_{t-h}^{t} \dot{x}^T(s)\bar{Z}\dot{x}(s)ds \end{aligned} \quad (15)$$

The next, by adding the right-hand side of (12) and (13) to $\dot{V}(x_t)$, equation (16) is derived (Appendix 3).

We also define (17) and (18):

$$\bar{\Xi} = \begin{bmatrix} \bar{P}\bar{A} + \bar{A}^T\bar{P} + \bar{Q} + \bar{h}X_{11} + N_1 + N_1^T + hA^TZA & \bar{P}\bar{B}K - \bar{N}_1 + \bar{N}_2^T + \bar{h}X_{12} + \bar{h}\bar{A}^T\bar{Z}\bar{B}K \\ * & -\bar{N}_2 + \bar{N}_2^T - \bar{Q} + \bar{h}K^TB^T\bar{Z}\bar{B}K \end{bmatrix} \quad (17)$$

$$\bar{\Psi} = \begin{bmatrix} X_{11} & X_{12} & \bar{N}_1 \\ * & X_{22} & \bar{N}_2 \\ * & * & \bar{Z} \end{bmatrix} \quad (18)$$

It can be seen from (16) that if it is $\Xi < 0, \Psi > 0$, then it is $\dot{V}(x_t) < 0$ and this means that the closed loop system of (8) is stable. The next, based on Lemma 1, $\Xi < 0$ can be easily provided in (19) (Appendix 3).

To obtain the K gain of the controller, it is necessary to use the following definitions:

$$\bar{L} = \bar{P}^{-1}, \bar{M}_1 = \bar{P}^{-1}\bar{N}_1\bar{P}^{-1}, \bar{M}_2 \doteq P^{-1}\bar{N}_2\bar{P}^{-1}, \bar{R} \doteq Z^{-1}, \bar{V} = K\bar{P}^{-1}, \bar{Q}_1 = P^{-1}\bar{Q}\bar{P}^{-1}, Y = diag\{\bar{P}^{-1}, \bar{P}^{-1}\}Xdiag\{\bar{P}^{-1}, \bar{P}^{-1}\}$$

By multiplying the right-hand and left-hand sides of (19) by $diag\{\bar{P}^{-1}, \bar{P}^{-1}, \bar{Z}^{-1}\}$, equation (20) is extracted (Appendix 3).

Obviously, equation (19) becomes equivalent to (9). Similarly, by multiplying the sides of (18) by $diag\{\bar{P}^{-1}, \bar{P}^{-1}, \bar{P}^{-1}\}$, equation (18) becomes equivalent to (10). Therefore, the proof of theorem 1 is completely finished.

According to the definition of Theorem 1, equation (10) can no longer be called an LMI due to the nonlinear conditions of $\bar{L}\bar{R}^{-1}\bar{L}$, therefore, it is not possible to use the convex optimization algorithm to search for the minimum value. For this reason, this paper uses cone complementarity linearization algorithm so that this algorithm is able to solve LMI [37]. Based on this, we can define the nonlinear optimization problem and its related constraints as (21) (Appendix 3).

In the following, according to the mentioned non-linear optimization process, the optimal gain matrix of the controller as well as the maximum value of the $\bar{h} = max(\tau)$ delay margin can be searched using the iterative algorithm proposed below.

Algorithm solution process:

Step 1: First, a small initial value for the delay margin should be chosen so that it can satisfy the feasibility region for (9) and (21).

Step 2: First, a set of possible matrix variable values should be set for $(\overline{L'}, \overline{L_1'}, \overline{V'}, \overline{M_1'}, \overline{M_2'}, \overline{F'}, \overline{F_1'}, \overline{Q_1'}, \overline{R'}, \overline{R_1'}, \overline{Y'})$, so that it satisfies (9) and (21), and then k = 0 is set.

Step 3: Solving the aforementioned nonlinear optimization problem with the constraints of LMIs in (9) and (21) and then setting:

$$\bar{F}_{k+1} = \bar{F}, F_{1,k+1} = \bar{F}_1, \bar{L}_{k+1} = \bar{l}, \bar{l}_{1,k+1} = \bar{L}_1, \bar{R}_{k+1} = \bar{R}, \bar{R}_{1,k+1} = \bar{R}_1.$$

Step 4: If the inequality (10) is possible, increase the scalar value h to a small amount and then return to step 2. Stop if inequality (10) is not feasible in a certain number of iterations. And otherwise, set step $k = k + 1$ and go to step 3.

Therefore, according to theorem 1 and the aforementioned algorithm, we will be able to obtain the optimal benefit of the feedback controller along with the maximum delay margin.

2.3. Observer-based state feedback design

In practical power systems, because the working state variables are not fully observed, it is usually preferred to use a feedback controller with measurable variables. Therefore, the state observer *Ob(s)* has been used to observe the state

variables unavailable for WAMS. In the present work, the mode observer based on normal pole placement is used in the design process [38]. In Fig. 1, the structure of the state observer in the WADC design is shown. In this case, the design process is done in two stages:

Step 1: determining a state feedback gain matrix for the desired poles of the system.

Step 2: determination of an observer's gain matrix for optimal placement of the observer's poles.

By combining the state space equations of the system and the observer equations and by defining the $e(t)$ error signal (difference between the actual and estimated signal), we will have (22):

$$\begin{bmatrix}\dot{x}(t)\\ \dot{e}(t)\end{bmatrix}=\begin{bmatrix}\bar{A}-\bar{B}\bar{K} & -\bar{B}\bar{K}\\ 0 & s\bar{I}-\bar{A}-\bar{L}\bar{C}\end{bmatrix} \quad (22)$$

Equation (22) describes the dynamics of a closed loop system with a state feedback controller and an observer. Therefore, the characteristic equation of the closed loop system is (23):

$$\begin{bmatrix}\bar{A}-\bar{B}\bar{K} & -\bar{B}\bar{K}\\ 0 & s\bar{I}-\bar{A}-\bar{L}\bar{C}\end{bmatrix}=0 \quad (23)$$

And as a result we will have (24):

$$|s\bar{I}-\bar{A}+\bar{B}\bar{K}||s\bar{I}+\bar{A}-\bar{L}\bar{C}| \quad (24)$$

Therefore, the closed loop poles of the state feedback control system with the observer are formed from the sum of the poles resulting from the state feedback design and the observer design. This means that the design of the observer and the positioning of the pole with mode feedback are done separately and independently from each other.

The desired poles of the closed loop (caused by the state feedback) are determined in such a way that the performance characteristics of the closed loop system are met. The poles of the observer are also determined in such a way that the response of the observer is much faster than the response of the system. A rule of thumb for determining the location of observer poles is to choose them in such a way that the response of the observer is 2 to 10 times faster than the response of the system. Therefore, in this paper, by forming state and observability matrices in MATLAB software, it is possible to obtain the sum of closed loop poles with state and observer feedback. Therefore, first, the closed loop poles of the system are extracted using the command $\bar{P}$=eig(A) in MATLAB software, and considering that we need the dynamics of the observer to be faster than the system itself, the poles of the observer must be at least 3 times farther from be the dominant poles of the system. Therefore, after obtaining the dominant poles of the system as P=eig(A) and placing these poles with a factor of 3 times farther from $\bar{P}$ as $\bar{P}_1$, the gain of the observer can be extracted using the $\bar{L}=place(\bar{A}',\bar{C}',\bar{P}_1)$ command.

In this paper, for gain K, we will have feedback according to the proposed controller and for gain L, we will have an observer in MATLAB software (Appendix 3).

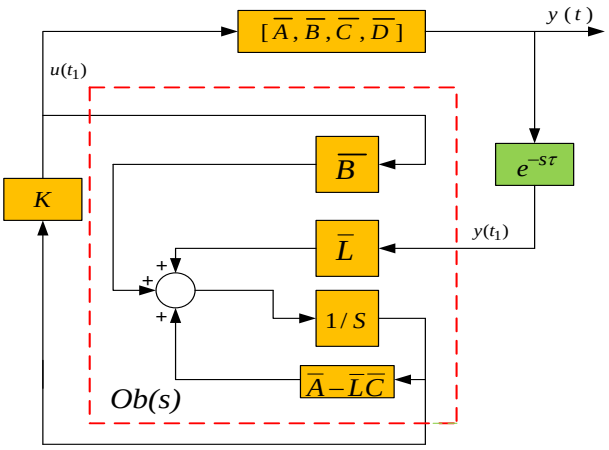

Fig. 1: Structure of state observer in WADC design for closed loop system.

3. THE SYSTEM UNDER OPERATION

According to Fig. 2, in this paper, the improved power system of 16 machines and 68 buses is used as a large-scale network for the performance of the proposed controller. For this purpose, the power system is connected to a DFIG-based wind farm equipped with SCESS through the SSSC compensator. The information of this network in connection with the parameters of transmission lines of synchronous generators and excitation system is reported in [38]. In the improved power system, the wind farm has a power of 100 MW, and in order to reduce wind fluctuations, a SCESS with a bidirectional converter is used in the DC link. According to the results of modal analysis in the power grid, between machines 10 and 14 there is an inter-area oscillatory mode with a frequency of 0.56 Hz and a damping ratio of 0.0165. For such LFO, WADC-based supplementary controller strategy for SSSC is better than injecting local signals. However, it should be noted that for effective application of WADC, appropriate wide feedback signals should be selected first. In this regard, based on the index JCOI [39], the power changes of P1-48 lines have a higher observability than the active power of other lines, so it has been used as a candidate for the stabilizing feedback signal to the WADC input. It should be noted that all synchronous generators are modeled with 5th order dynamic model, wind unit with 4th order model, SCESS unit with 2nd order and SSSC modeled with 2nd order. By specifying the input vector $U=[\Delta V_R, \Delta X_F]$ and the output vector$Y=[\Delta E_{fd}, \Delta\alpha_{se}]$, the system model can be reduced to order 13 using the *schmr* reduction model. For this purpose, the *schmr* function in the Robust MATLAB Simulink toolbox was used [36]. It is worth mentioning that local PSS is installed on generators (G_1, G_4, G_8, G_9, G_{12}, G_{13}, G_{14}, G_{15}, G_{16}) by default. For the purpose of comparison, in addition to the design of the WADC controller, the classical power oscillation damping (CPOD) controller with PL input (specified in Fig. 2) has been used as a local signal in the SSSC. This controller has no time delay because it is fed through the local signal.

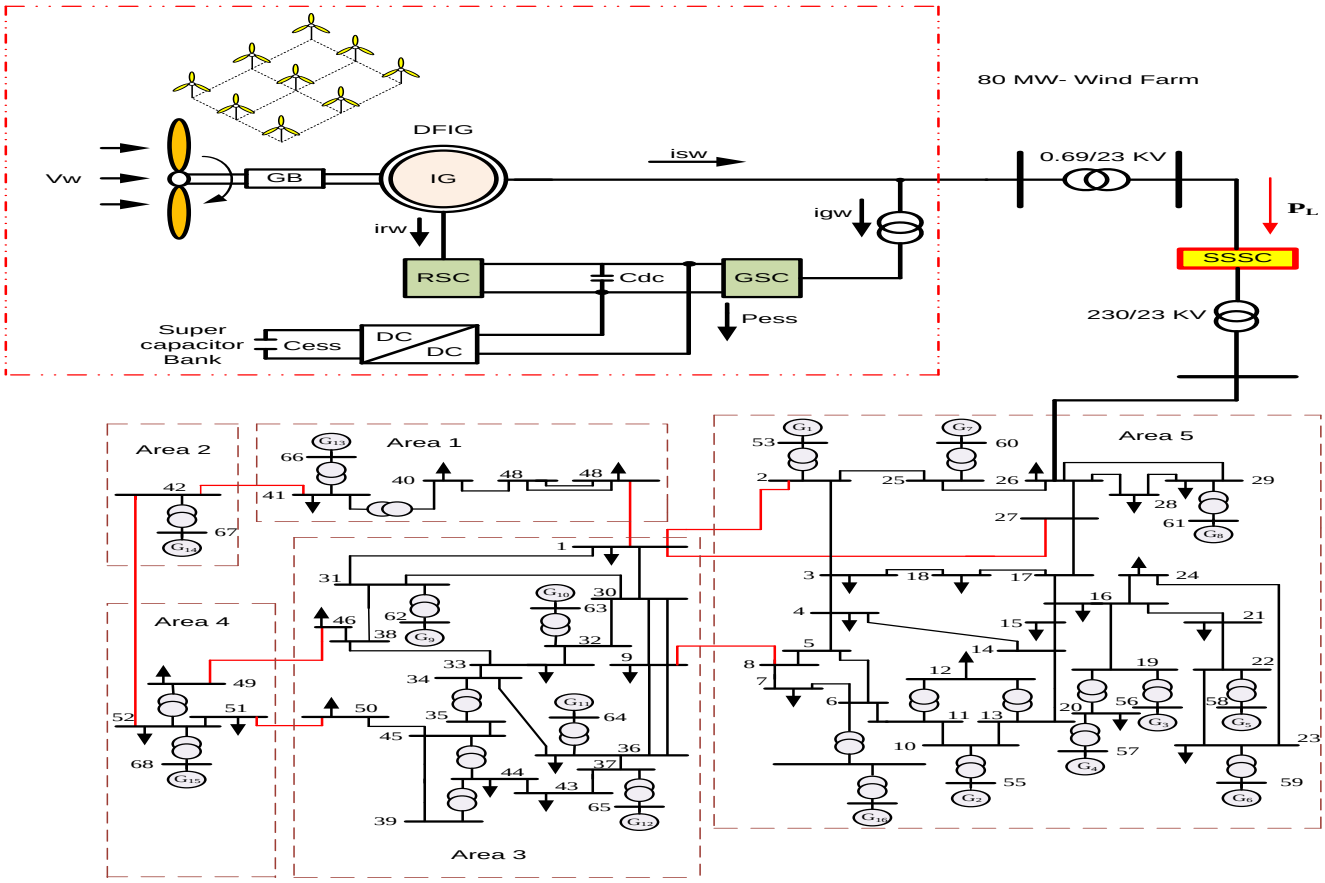

Fig. 2: Single-line diagram of the power system under study.

3.1. Modeling of the Elements Related to the Power System Under Study

3.1.1. Synchronous generator model

In this part, in order to analyze the dynamic equations of SG, the two-axis model is used [40]. In this model, the effects of sub-transient reactances are ignored and only the transient reactances of the synchronous generator are used in the modeling. Based on this, the dynamic equations of the biaxial model for the i-th SG can be expressed as (25):

$$\begin{cases} \dfrac{dE'_{qi}}{dt} = \dfrac{1}{T'_{doi}}[-E'_{qi} + E_{fdi} + (X_{di} - X'_{di})]I_{di} \\ \dfrac{dE'_{di}}{dt} = \dfrac{1}{T'_{qoi}}\left[-E'_{di} - \left(X_{qi} - X'_{qi}\right)I_{qi}\right] \\ \dfrac{dE_{fdi}}{dt} = \dfrac{-1}{T_{Ei}}[E_{fdi}(K_{Ei} + S_{Ei}(E_{fdi})) - V_{Ri}] \\ \dfrac{d\omega_i}{dt} = \dfrac{1}{\tau_{ji}} \times \\ [T_{mi} - \left[I_{di}E'_{di} + I_{qi}E'_{qi} - \left(L'_{qi} - L'_{di}\right)I_{di}I_{qi} + D_i\omega_i\right] \\ \dfrac{d\delta_i}{dt} = \omega_i - \omega_s \end{cases} \quad (25)$$

3.1.2. DFIG descriptive model

As can be seen from Fig. 3, the DFIG unit connects the RSC and GSC converters back to back through the dc link, and its task is to maintain the power balance between the converters. In the present work, vector method is used for DFIG dynamic modeling [40]. Based on the equations of voltage and leakage flux in the induction generator, the state equations for the rotor and stator currents in the d-q reference frame can be described as (26) (Appendix 3).

In (26) it is $H = \omega_b.\left(L_{mm}^2 - L_{ss}.L_{rr}\right)^{-1}$.

3.1.3. SCESS converter controller

In this pipe, a SCEES has been used in order to fully ensure that the DC link voltage is maintained in the air unit. The circuit structure of SCESS is shown in Fig. 4. The SCESS structure includes a capacitor bank and a two-switch DC/DC converter that is connected to the DFIG through a DC link. DC/DC converter can be used in BOOST and BUCK modes depending on S_1 and S_2 switches.

It can be seen from Fig. 4 that the SCESS converter has two switches S_1 and S_2 along with an inductor and energy storage [32].

According to the average value of the dynamic model, the output current of this converter is equal to (27):

$$\begin{cases} \dfrac{di_{sc}}{dt} = \dfrac{1}{L_S}\left(V_{SC} - f_S V_{DC} - R_{\ S} i_{SC}\right) \\ i_{SC\_DC} = f_S i_{SC} \end{cases} \quad (27)$$

In which, if it is $f_S = D_S$, the converter will work in Buck mode, and if it is $f_S = 1 - D_S$, the converter will work in Boost mode. According to the equivalent circuit in Fig.4, the dc link voltage is equal to (28):

$$\begin{cases} \dfrac{dV_{C_{SC}}}{dt} = \dfrac{1}{C_{SC}}(-i_{SC} - \dfrac{V_{C_{SC}}}{R_{p_{SC}}}) \\ V_{SC} = V_{C_{SC}} - R_{S_{SC}} i_{SC} \end{cases} \quad (28)$$

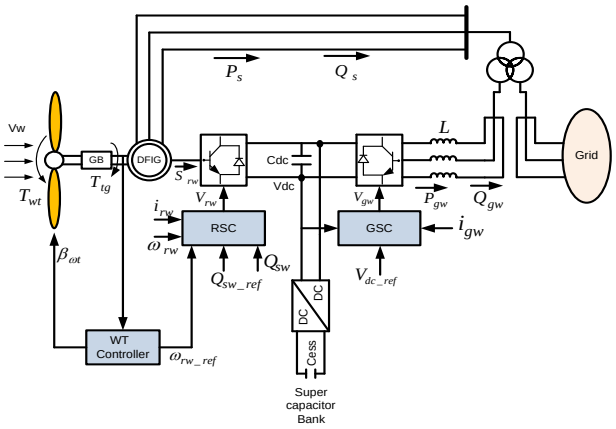

Fig. 3: Diagram of DFIG-based wind turbine.

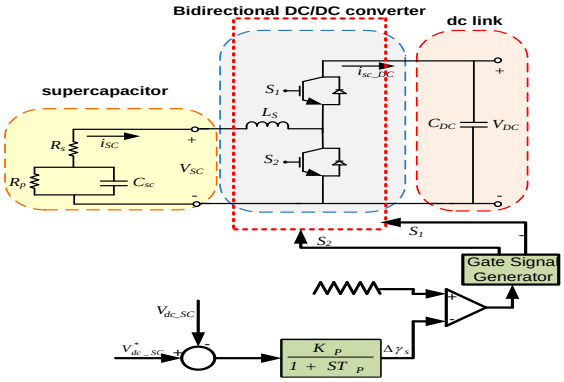

Fig. 4: Control block diagram for SCESS.

3.1.4. *SSSC Mathematical Model*

The SSSC is used as a voltage source converter (VSC) in both inductive and capacitive modes for compensating reactive power in the transmission line. The circuit structure of this type of FACTS is shown in Fig. 5. In SSSC circuit structure, a VSC, a series transformer, a capacitor with C_{dc} capacity and a controller are used. Using the synchronous reference frame, the series injection voltage in SSSC can be described by (29) in the d-q axis [41]:

$$\begin{cases} v_{ds} = m_c Z_{inv} V_{dc\_sssc} Cos(\alpha_{se}) \\ v_{qs} = m_c Z_{inv} V_{dc\_sssc} Sin(\alpha_{se}) \end{cases} \quad (29)$$

In (29), α_{se} is the phase angle of the injection voltage, mc is the conversion ratio of the coupling transformer and Z_{inv} is the constant of the inverter, which is related to the voltage of the dc side over the line-phase voltage of the ac side. The dynamic equation of the DC link capacitor in order to maintain the power balance on the dc and ac sides is expressed by (30):

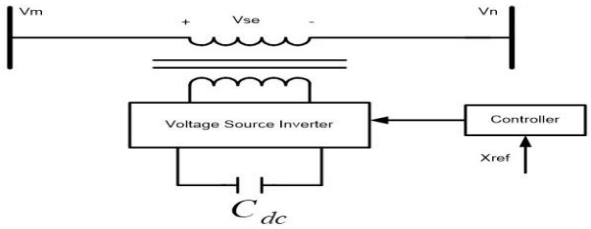

Fig. 5: One-line diagram of a SSSC.

$$\frac{dV_{dc\_sssc}}{dt} = \frac{1}{C_{dc}}\left[m_c Z_{inv}(i_d \cos\alpha_{se} + i_q \sin\alpha_{se})\right] - \frac{V_{dc\_sssc}}{C_{dc}.R_{dc}} \quad (30)$$

The control block diagram of SSSC for the capacitor mode along with the damping controller is shown in Fig. 6. In this structure, by adding a control signal based on X_F, inter-area fluctuations in the power system can be damped through WADC or CPOD.

4. SIMULATION RESULTS

The structure of the closed loop system for simulations is shown in Fig. 7. In this structure, the loops related to the controllers and how they are related to the power system is specified. All the control loops including the SSSC converter control loop along with the damping control loop, the SCESS converter control loop and the DFIG control loops in the RSC and the GSC are connected to each other through the DC link. The simulation results have been evaluated in the form of four scenarios, so that in this evaluation, the wind pattern for all four scenarios is according to Fig.8. The SG excitation system is IEEE-1 type, the details of which are reported in [42].

4.1. First scenario

In this scenario, we apply a three-phase short-circuit fault temporarily for 0.1 second near bus 11 (between lines 11-12). Accordingly, in Figs. 9a and 9b, respectively, the changes in the output power of the wind unit and the response of the active power of line 1-48 are shown by applying a time delay of 100ms in sending remote signals to the WADC. It can be seen from the results of this response, even if there is a time delay, the WADC controller provides better stability than the CPOD method. Also, in Figs. 9c and 9d, the DC voltage of SSSC and the reactive power changes of the inter-area line 1-27 per time delay of 100ms are shown, respectively. From the results of this scenario, it can be seen that the proposed controller for damping power fluctuations has a favorable performance against uncertainties caused by time delay and three-phase fault. This improvement is clearly seen both in the settling time and in overshoot and undershoots.

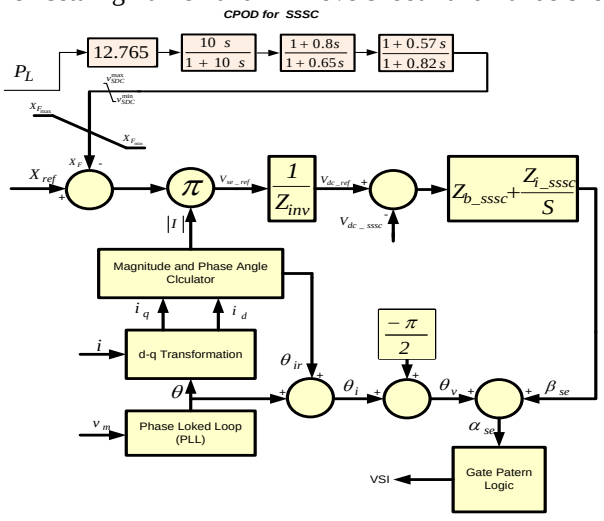

Fig. 6: The proposed damping controller structure for a SSSC.

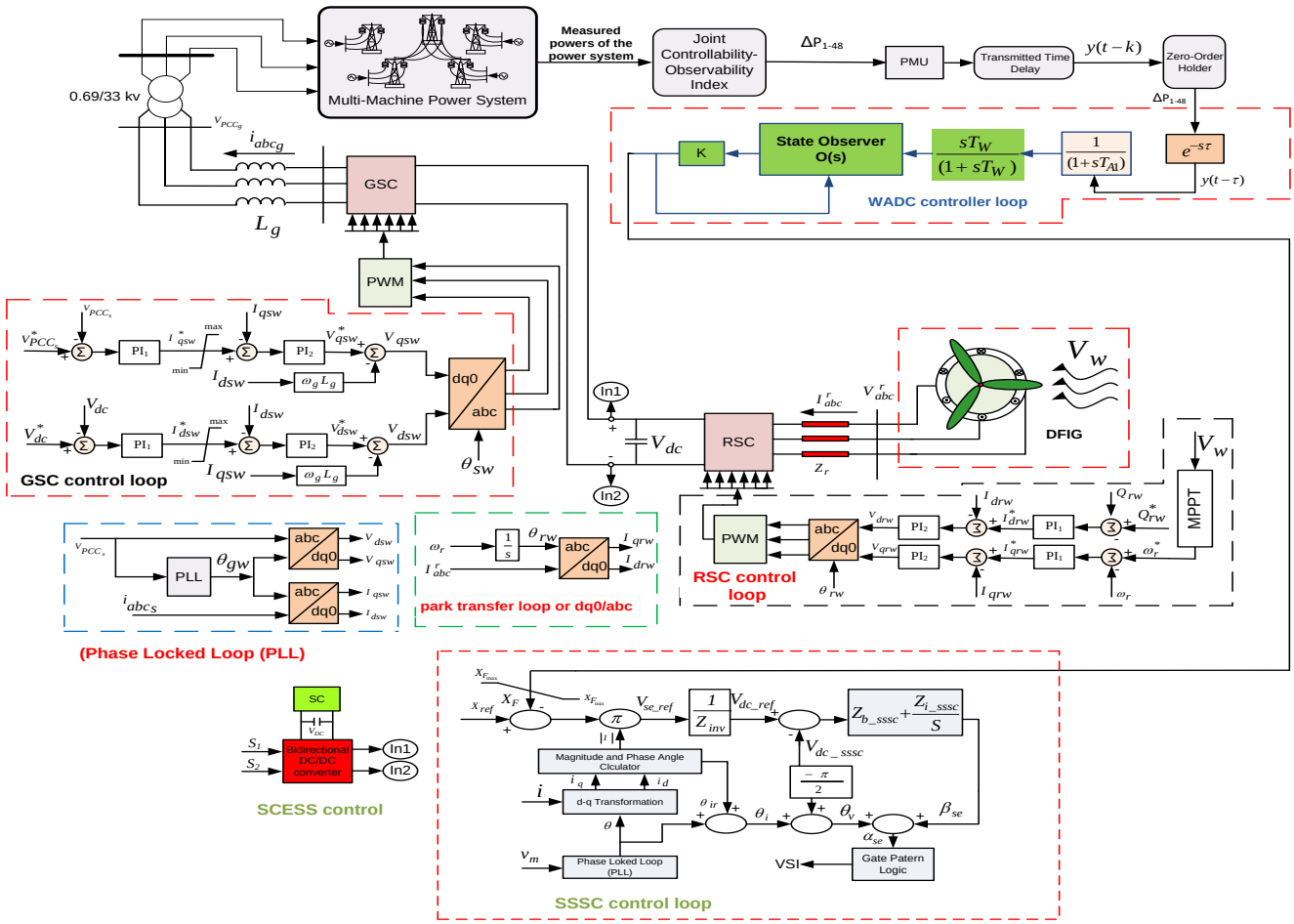

Fig. 7: The closed loop system of the proposed controller along with all the control loops of the converters.

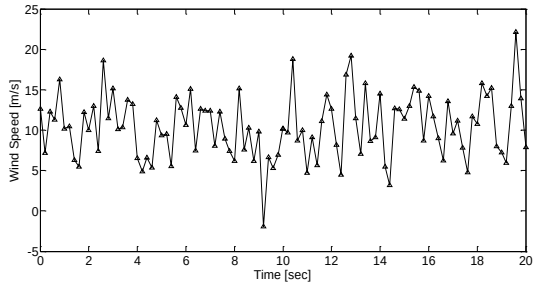

Fig. 8: Wind variation for DFIG unit.

4.2. Second scenario

In this scenario, a three-phase fault occurred permanently near bus 31 (between line 31 and 38) within 2 seconds, and because the fault was not resolved after 0.1 second, line 31-38 was outage. In addition, by changing the input mechanical power of the generators (G_1, G_4, G_8, G_{10}, G_{12}) by +10% and considering the wind pattern as in the first scenario, the simulation results have been evaluated. Based on this, the speed deviation of generators 6-14 in Fig.10 (a), the power changes of line 14-15 in Fig.10 (b), the SSSC output power in Fig.10(c), as well as the power changes of line 8-9 in Fig.10 (d) is shown for time delays of 300ms. From these results of this scenario, it is clearly seen that the proposed controller is optimal under any conditions and provides the desired stability for the system. If in the case without a controller, the oscillations caused by uncertainties are not well damped and the stability of the system decreases with the passage of time.

4.3. Third scenario

In this scenario, in order to operate with greater uncertainty, step changes have been made on the load connected to bus 26 of the power system. Thus: in 5 seconds, the amount of load increased from 3.5 to 4.82, and in 12 seconds, it decreased from 3.82 to 2.22, and again in 25 seconds, it increased from 2.22 to 5.3. The details of these changes are shown in Fig. 11a. It should be noted that the wind speed for the wind farm increases from 11 m/s to 12 m/s with increasing load and decreases from 12 m/s to 11 m/s with decreasing load. In addition, a time delay of 200 milliseconds in 5 seconds is considered for WADC. Figs. 11b and 11c show the speed deviation response of G9-10 and G6-8 for load changes. So that WADC has been able to control and dampen the deviations well at different moments with its accurate performance during load change. The response of changes in active power between buses 41-42 is shown in Fig. 11d, as well as changes in reactive power of the wind unit in Fig. 11e. In this figure, with load reduction in 5 seconds, first the power between lines increased, and with load increase in 12 seconds, the amount of power between lines decreased, and then with load reduction in 25 seconds, the amount of power flow in lines increased. Also, the input attenuation signal for SSSC by the proposed controller is shown in Fig. 11f. According to the results obtained in this scenario, the robustness of the proposed controller under rapid changes in power compared to the CPOD controller has been well demonstrated.

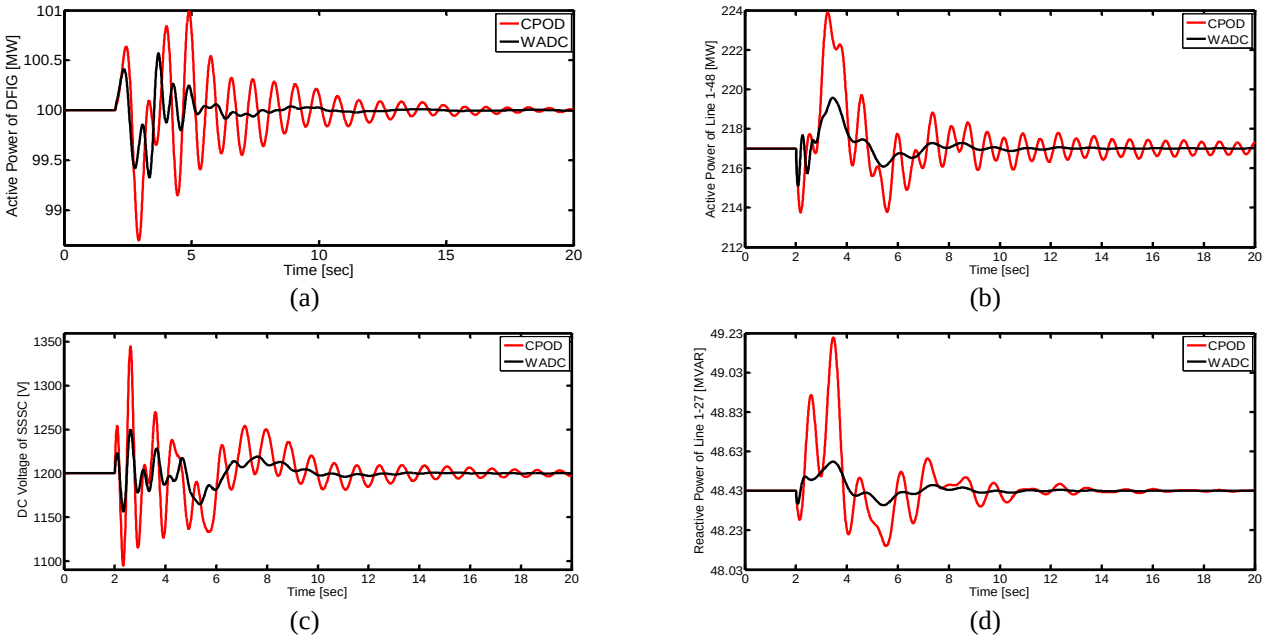

Fig. 9: Response results related to scenario 1.

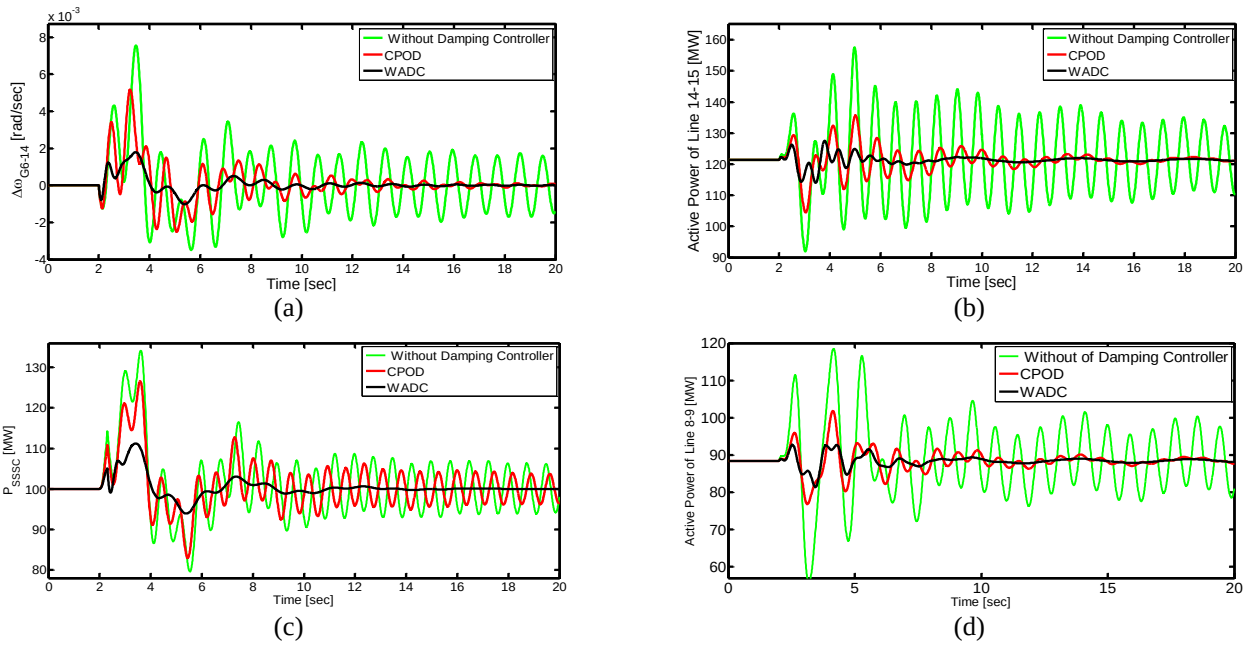

Fig. 10: Response results related to scenario 2.

4.4. Fourth scenario: Case comparison with other methods and discussion and analysis

In this section, in order to show the better performance of the proposed controller compared to references [22, 23], the simulation results have been analyzed. Therefore, by applying a permanent three-phase short-circuit fault in 2 seconds near bus 2 (between line 2 and 3), line 2-3 is outage after 0.1 second due to the fault not being resolved. The pattern of wind blowing and solar radiation is the same as the first scenario and the change in the input mechanical power of the generators (G_1, G_5, G_{11}, G_{40}) is considered to be +15%. Based on this, Figs .12a and 12b show the changes of active power between line 42-52 and DC voltage of SCESS per time delay of 300ms, respectively. From these figs, it can be seen that the improvement of oscillation damping in the proposed method is much more favorable and faster than the other two references, which has led to the reduction of settling time, overshooting and undershooting. Figs. 12c and 12d show the changes in the active power of the wind unit for the presence and absence of SSSC and SCESS units, respectively. From these figures, it can be seen that due to the outage, each unit is affected by the power grid, wind farm power and SSSC power, which leads to a decrease in the stability of the power system. This is despite the fact that in the presence of SSSC and SCESS units, even if there are time delays of 300 milliseconds at the WADC input, a much more favorable damping is provided than without them. Therefore, the effect of SSSC and SCESS in connecting to the power system and DC link is very important, so that the power fluctuations of renewable units can be improved through these units. In Figs. 12a and 12b, it can be seen that the presence of a fault leads

to changes in the active power and DC voltage of the storage system to more than 5%, which by applying a time delay of 300 milliseconds, the amplitude and cycle of oscillations for the proposed method, reference [22] and [23] is about 8.2, 14.7 and 16.6. It can be seen in Figs. 12c and 12d that if SSSC and SCESS are used alone to compensate the network stability, the existence of fluctuations caused by delay and disturbances lasts for more than 15 seconds. Therefore, the overshoot and undershoot will be more than 5%, which will not be a good number to maintain optimal stability. But with the optimal design of SSSC together with SCESS, it is possible to reduce the amount of overshoot and undershoot to below 5%, after which the average settling time is reduced to less than 8.476 seconds.

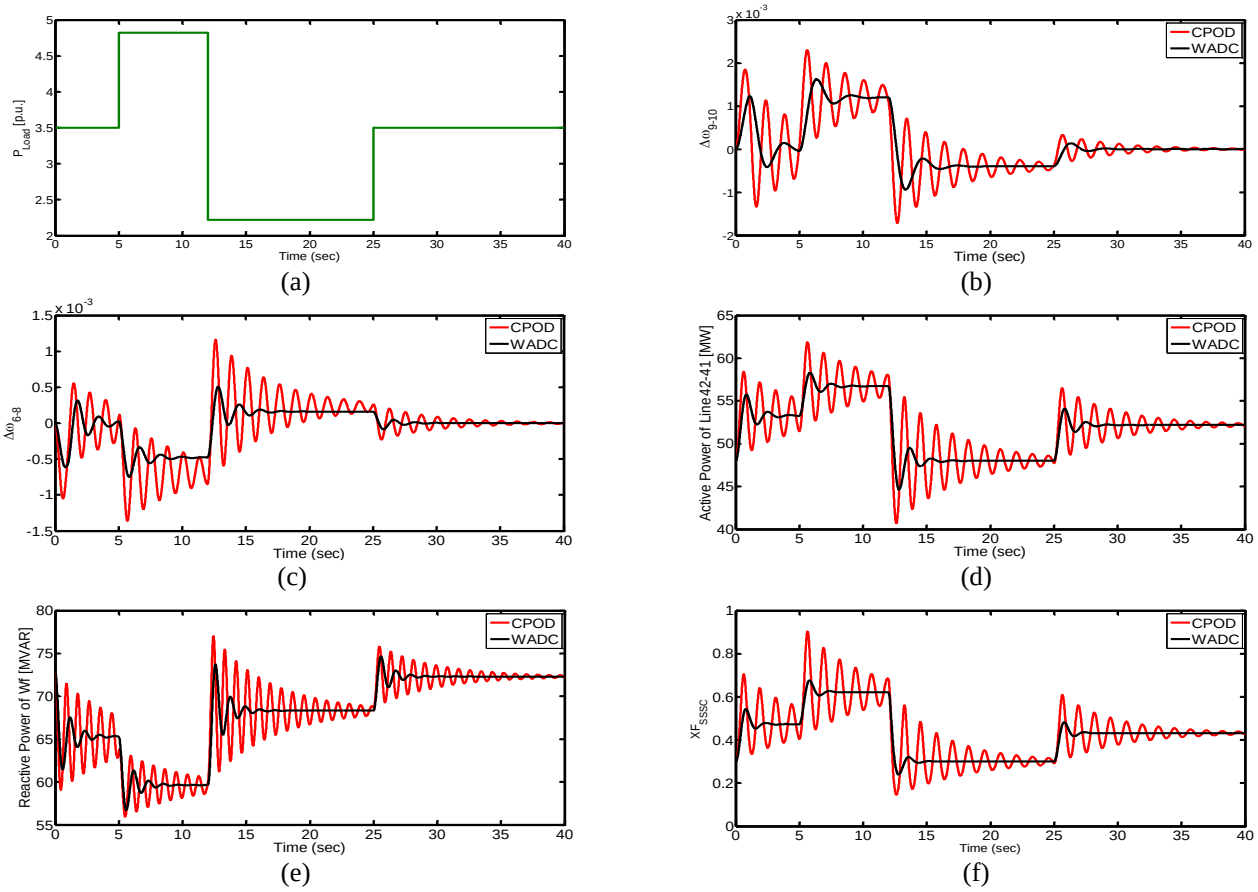

Fig. 11: Response results related to scenario 3.

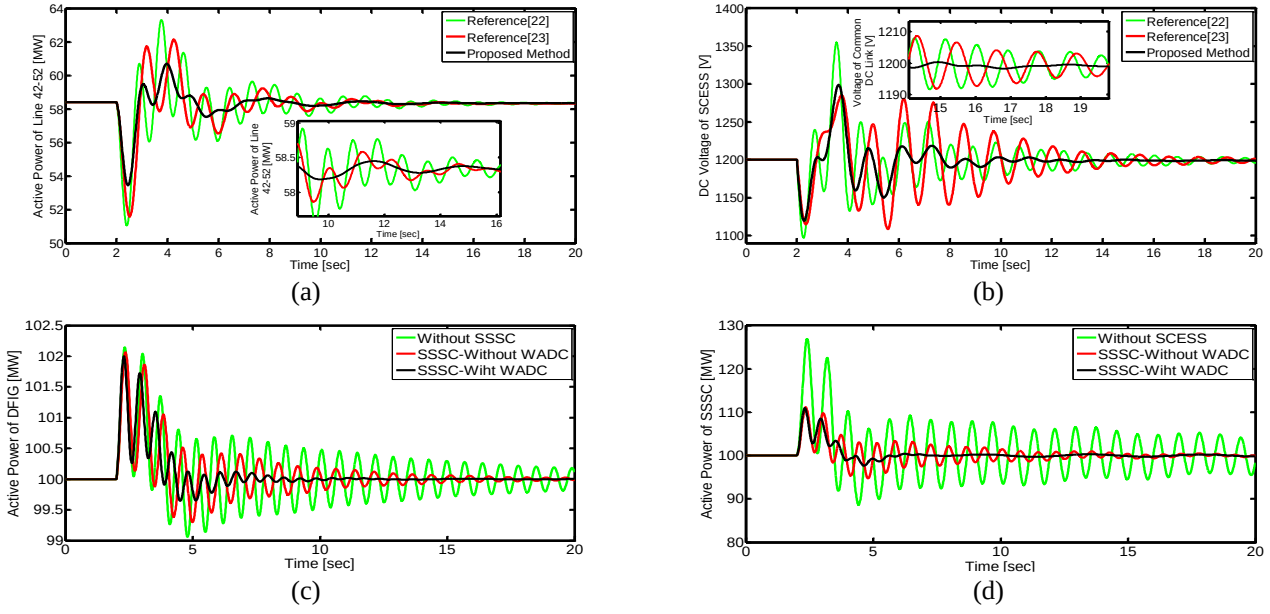

Fig. 12: Response results related to scenario 4.

5. CONCLUSION

In this paper, with the design of the WADC controller, the stability of the power system was evaluated using the FWM method under different scenarios. The FWM design method is solved by introducing a set of nonlinear matrix inequality constraints based on LMI constraints in the form of an optimization problem. In this method, by introducing the non-linear optimization algorithm, it can be used to search for the most optimal gain matrix and the maximum delay margin of the control signal. This design process is able to avoid the destructive effect of large amplitude time delays on the performance of the power system. Finally, the damping signal of the WADC controller was applied using the proposed method as a supplementary signal to the SSSC converter to reduce low frequency oscillations. The simulation results were tested on the improved power system of 16 -machines using MATLAB software. From the results of this simulation, it is clearly seen that in the proposed method, in addition to improving the stability of the power system, the changes caused by time delays in sending signals from far away can be well controlled.

In summary, it can be said that in the proposed method, the average settling time for scenarios 1 and 2 is 8.2 and 8.8 seconds, respectively. Meanwhile, in these scenarios, the average sitting time for the classic CPOD method is equal to 18.5 and 19.65 seconds, respectively. In scenario 3, the overshoot and undershoot values for the proposed method and CPOD are equal to (2.567% and 1.996%) and (5.765% and 4.873%) respectively. In the same way, in scenario 4, the average settling time, overshoot and undershoot compared to the methods in [22] and [23] are equal to (8.476 seconds, 2.328% and 2.096%), respectively (14.532 seconds and 4.842% and 3.559%) and (16.956 seconds and 4.389% and 3.994%) have been obtained. Based on this, it can be seen that the proposed method has been of great help in improving of the settling time, overshoot and undershoot of fluctuations.

APPENDICES

Appendix 1. Adapting the proposed method to the studied power system

This part of matching the proposed controller with the dynamic model of the system includes: synchronous machines [40], wind power plant [40], BESS [42] and SSSC [41]. Therefore, for the closed loop system of (6), X is the state vector of the system, U is the input vector, and Y is the output state vector, which are defined in this paper as follows:

$$\begin{cases} X = [\Delta i_{dsw}, \Delta i_{qsw}, \Delta i_{drw}, \Delta i_{qrw}, \Delta E'_d, \Delta E'_q, \Delta E_{fd}, \Delta\delta \\ \qquad , \Delta\omega, \Delta i_{SC}, \Delta V_{C_{SC}}, \Delta\alpha_{se}, \Delta V_{dc\_sssc}]^T \\ U = [\Delta V_R, \Delta X_F] \\ Y = [\Delta E_{fd}, \Delta\alpha_{se}] \end{cases}$$

For the above vectors we will have:

$\Delta i_{dsw}, \Delta i_{qsw}, \Delta i_{drw}, \Delta i_{qrw}$: Corresponding to the stator and rotor currents of the wind unit in d and q axes, respectively.

$\Delta E_d^{'}, \Delta E_q^{'}$: Corresponding to the electromotive force voltage of synchronous generators in d and q axes, respectively.

$\Delta E_{fd}, \Delta\delta, \Delta\omega, \Delta V_R$: Respectively related to excitation field voltage, rotor angle, rotor speed and supplementary signal of PSS controller in synchronous generators [43].

$\Delta i_{SC}, \Delta V_{C_{SC}}, \Delta\alpha_{se}$: Respectively related to the current, voltage and switching signal of the PWM converter in the BESS control loop.

ΔV_{dc_sssc}: SSSC compensator dc voltage.

ΔX_F: Supplementary damping controller signal sent through WADC to SSSC.

The values of matrices A, B and C are equal to:

$$A = \begin{bmatrix} 1.2435 & 0.5671 & 0.1256 & 0.9801 & 0.3451 & 1.7654 & 0.4056 & 0.5674 & 0.7658 & 0.2345 & 0.6547 & 1.2087 & 0.5187 \\ 0.4062 & 0.6134 & 1.8964 & 0.9380 & 0.5438 & 0.3275 & 0.5610 & 0.7403 & 1.5021 & 0.6581 & 0.8055 & 0.4328 & 0.6004 \\ 0.7630 & 0.6543 & 0.6754 & 1.4571 & 1.5430 & 0.5611 & 0.1134 & 1.3267 & 1.2278 & 0.1087 & 1.5670 & 0.4328 & 0.5611 \\ 1.3335 & 1.6533 & 0.7641 & 0.8904 & 1.8601 & 1.7773 & 0.8765 & 0.7653 & 0.4455 & 0.7655 & 0.6531 & 0.7004 & 0.7432 \\ 0.4033 & 0.5427 & 1.6187 & 1.5890 & 0.9403 & 0.8126 & 1.2864 & 0.4243 & 0.5679 & 0.5428 & 0.6541 & 0.6507 & 1.4506 \\ 0.6643 & 0.6782 & 0.8439 & 0.7901 & 1.8404 & 0.8175 & 0.5602 & 1.7632 & 0.8922 & 0.9027 & 0.8900 & 0.9764 & 0.9654 \\ 0.8765 & 0.5431 & 1.7654 & 1.8612 & 0.4428 & 0.5670 & 1.4321 & 1.6643 & 0.8754 & 1.6540 & 0.6543 & 1.4328 & 0.7654 \\ 0.5432 & 0.6704 & 0.4328 & 0.8953 & 1.7654 & 0.2109 & 0.5130 & 0.1986 & 0.2687 & 0.4356 & 1.7521 & 0.6705 & 1.7608 \\ 0.5631 & 0.1778 & 0.5899 & 0.4332 & 0.6477 & 0.6728 & 0.8769 & 0.6654 & 1.1345 & 0.2876 & 0.5431 & 0.7567 & 0.8876 \\ 0.4332 & 0.6088 & 1.4328 & 0.8601 & 0.7754 & 0.8658 & 1.4458 & 1.7765 & 0.3322 & 0.5548 & 0.8876 & 1.6654 & 1.8904 \\ 0.6367 & 1.8654 & 0.6784 & 1.0876 & 0.5567 & 0.7439 & 0.8992 & 0.9701 & 1.0677 & 0.9978 & 0.3379 & 0.5543 & 0.8327 \\ 1.0408 & 0.6648 & 0.3972 & 0.6520 & 1.1390 & 0.7694 & 0.4861 & 0.3863 & 0.8129 & 0.9411 & 0.6034 & 1.4561 & 0.8750 \\ 0.6276 & 0.5399 & 0.6499 & 0.6781 & 0.7892 & 0.8904 & 0.7432 & 0.7894 & 0.6432 & 0.8902 & 1.432 & 1.167 & 0.6571 \end{bmatrix}$$

$$B = \begin{bmatrix} 0 & 0 & 0 & 0 & 0 & 0 & 0.9765 & 0 & 0 & 0 & 0 & 0 & 0 \\ 0 & 0 & 0 & 0 & 0 & 0 & 0 & 0 & 0 & 0 & 0.8765 & 0 \end{bmatrix}$$

$$C = \begin{bmatrix} 0 & 0 & 0 & 0 & 0 & 0 & 0.6543 & 0 & 0 & 0 & 0 & 0 & 0 \\ 0 & 0 & 0 & 0 & 0 & 0 & 0 & 0 & 0 & 0 & 0.9501 & 0 \end{bmatrix}$$

Appendix 2. The information related to the controller parameters is reported in Table 1.

Table 1: Information about controllers and parameters related to them.

Information about the BESS along with the controllers related to it			
R_s=0.1 Ω	R_p=0.04 Ω	L_s=4.5 mH	C_{sc}=75μf
T_W=10	T_{A1}=2.45	K_{pf}=6.65	K_{if}=3.15
K_{pg}=6.65	K_{ig}=6.65	(switching frequency) f=5 KH	
Information about DFIG controllers			
PI_1:K_{p1}=4.65,K_{i1}=1.51	PI_2:K_{p2}=6.43,K_{i2}=2.32	$R_g+j\omega L_g$=0.86+j0.054ωΩ	$R_g+j\omega L_g$=0.22+j.0.18ωΩ

Appendix 3. Equations (16), (19), (20), (21), (26) and gain K and gain L, which were used in this paper are defined as follows:

$$\dot{V}(x_t) = x^T(t)[\bar{P}\bar{A} + \bar{A}^T\bar{P}]x(t) + 2x^T(t)\bar{P}\bar{B}Kx(t_1) + x^T\bar{Q}x(t) - x^T(t_1)\bar{Q}x(t_1) + h[\bar{A}x(t) + \bar{B}Kx(t_1)]^T$$
$$\bar{Z}[\bar{A}x(t) + \bar{B}Kx(t-\tau)] + \bar{h}\bar{\xi}^T(t)X\bar{\xi}(t) + 2(x^T(t)\bar{N}_1 + x^T(t_1)\bar{N}_2)[x(t) - x(t_1)] - \int_{t_1}^{t}\dot{x}^T(s)\bar{Z}\dot{x}(s)ds$$
$$-\int_{t_1}^{t}\bar{\xi}^T(t)X\bar{\xi}(t)ds - 2[x^T(t)\bar{N}_1 + x^T(t_1)\bar{N}_2]\int_{t_1}^{t}\dot{x}(s)ds = x^T(t)[\bar{P}\bar{A} + \bar{A}^T\bar{P} + \bar{h}\bar{A}^T\bar{Z}\bar{A} + \bar{Q} + \bar{h}X_{11} + \bar{N}_1 + \bar{N}_1^T]x(t)$$
$$+x^T(t)[\bar{P}\bar{B}K + \bar{h}\bar{A}^T\bar{Z}\bar{B}K - \bar{N}_1 + \bar{N}_2^T + \bar{h}X_{12}]^T x(t_1) + x^T(t_1)[\bar{P}\bar{B}K + \bar{h}\bar{A}^T\bar{Z}\bar{B}K - \bar{N}_1 + \bar{N}_2^T + \bar{h}X_{12}]^T x(t)$$
$$+x^T(t_1)[-\bar{N}_2 - \bar{N}_2^T - \bar{Q} + \bar{h}X_{22} + \bar{h}K^T\bar{B}^T\bar{Z}BKX_{12}]x(t_1)$$
$$-\int_{t_1}^{t}[\dot{x}^T\bar{Z}\dot{x}(s) + \bar{\xi}^T(t)X\bar{\xi}(t) + 2(x^T(t)\bar{N}_1 + x^T(t_1)\bar{N}_2)\dot{x}(s)]\,ds = \tag{16}$$
$$\begin{bmatrix} x(t) \\ x(t-\tau) \end{bmatrix}^T \begin{bmatrix} \bar{P}\bar{A} + \bar{A}^T\bar{P} + \bar{Q} + \bar{h}X_{11} & \bar{P}\bar{B}K - \bar{N}_1 + \bar{N}_2^T \\ +N_1 + N_1^T + hA^TZA & +\bar{h}X_{12} + \bar{h}\bar{A}^T\bar{Z}\bar{B}K \\ * & -\bar{N}_2 + \bar{N}_2^T - \bar{Q} \\ & +\bar{h}K^TB^T\bar{Z}\bar{B}K \end{bmatrix} \times \begin{bmatrix} x(t) \\ x(t_1) \end{bmatrix}^T$$
$$\int_{t_1\tau}^{t} \begin{bmatrix} x(t) \\ x(t_1) \\ \dot{x}(s) \end{bmatrix}^T \times \begin{bmatrix} X_{11} & X_{12} & \bar{N}_1 \\ * & X_{22} & \bar{N}_2 \\ * & * & \bar{Z} \end{bmatrix} \begin{bmatrix} x(t) \\ x(t_1) \\ \dot{x}(s) \end{bmatrix} ds$$

$$\bar{\Xi} = \begin{bmatrix} \bar{P}\bar{A} + \bar{A}^T\bar{P} + \bar{Q} + \bar{h}X_{11} + \bar{N}_1 + \bar{N}_1^T & \bar{P}\bar{B}K - \bar{N}_1 + \bar{N}_2^T + \bar{h}X_{12} & \bar{h}\bar{A}^T\bar{Z} \\ * & -\bar{N}_1 + \bar{N}_2^T - \bar{Q} + \bar{h}X_{22} & \bar{h}\bar{K}^T\bar{B}^T\bar{Z} \\ * & * & -\bar{h}\bar{Z} \end{bmatrix} < 0 \tag{19}$$

$$\Xi = \begin{bmatrix} \bar{P}^{-1} & 0 & 0 \\ 0 & \bar{P}^{-1} & 0 \\ 0 & 0 & \bar{Z}^{-1} \end{bmatrix} \begin{bmatrix} \bar{P}\bar{A} + \bar{A}^T\bar{P} + \bar{Q} + \bar{h}X_{11} + \bar{N}_1 + \bar{N}_1^T & \bar{P}\bar{B}K - \bar{N}_1 + \bar{N}_2^T + \bar{h}X_{12} & \bar{h}\bar{A}^T\bar{Z} \\ * & -\bar{N}_1 + \bar{N}_2^T - \bar{Q} + \bar{h}X_{22} & \bar{h}\bar{K}^T\bar{B}^T\bar{Z} \\ * & * & -\bar{h}\bar{Z} \end{bmatrix}$$
$$\times \begin{bmatrix} \bar{P}^{-1} & 0 & 0 \\ 0 & \bar{P}^{-1} & 0 \\ 0 & 0 & \bar{Z}^{-1} \end{bmatrix} = \begin{bmatrix} \bar{A}\bar{L} + \bar{L}\bar{A}^T + \bar{Q}_1 + \bar{h}Y_{11} + \bar{M}_1 + \bar{M}_1^T & \bar{B}\bar{V} - \bar{M}_1 + \bar{M}_2^T + \bar{h}Y_{12} & \bar{h}\bar{L}\bar{A}^T \\ * & -\bar{M}_2 - \bar{M}_2^T - \bar{Q}_1 + \bar{h}Y_{22} & \bar{h}\bar{V}^T\bar{B}^T \\ * & * & -\bar{h}\bar{R} \end{bmatrix} < 0 \tag{20}$$

$$Minimize \quad tr\{\bar{F}\bar{F}_1 + \bar{L}\bar{L}_1 + \bar{R}\bar{R}_1\}$$
$$Subject \quad to:$$
$$\begin{bmatrix} \bar{A}\bar{L} + \bar{L}\bar{A}^T + \bar{Q}_1 + \bar{h}Y_{11} + \bar{M}_1 + \bar{M}_1^T & \bar{B}\bar{V} - \bar{M}_1 + \bar{M}_2^T + \bar{h}Y_{12} & \bar{h}\bar{L}\bar{A}^T \\ * & -\bar{M}_2 - \bar{M}_2^T - \bar{Q}_1 + \bar{h}Y_{22} & \bar{h}\bar{V}^T\bar{B}^T \\ * & * & -\bar{h}\bar{R} \end{bmatrix} < 0$$
$$\begin{bmatrix} Y_{11} & Y_{12} & \bar{M}_1 \\ * & Y_{22} & \bar{M}_2 \\ * & * & \bar{F} \end{bmatrix} > 0 \tag{21}$$
$$\begin{cases} \begin{bmatrix} \bar{F} & \bar{I} \\ \bar{I} & \bar{F}_1 \end{bmatrix} > 0, \begin{bmatrix} \bar{F}_1 & \bar{L}_1 \\ \bar{L}_1 & \bar{R}_1 \end{bmatrix} > 0 \\ \bar{L} > 0, \bar{F} > 0, \bar{R} > 0 \end{cases}$$

$$\begin{cases} \dfrac{di_{dsw}}{dt} = H[R_s L_{rr} i_{dsw} + ((\omega_s - \omega_r).L_{mm}^2 - \omega_s L_{rr} L_{ss}) i_{qsw} - R_r L_{mm} i_{drw} - \omega_r L_{rr} L_{mm} i_{qrw} + L_{mm} V_{drw} - L_{rr} V_{dsw}] \\ \dfrac{di_{qsw}}{dt} = H[(-(\omega_s - \omega_r).L_{mm}^2 + \omega_s L_{rr} L_{ss}) i_{dsw} + R_s L_{rr} i_{qsw} + \omega_r L_{rr} L_{mm} i_{drw} - R_r L_{mm} i_{qrw} + L_{mm} V_{qrw} - L_{rr} V_{qsw}] \\ \dfrac{di_{drw}}{dt} = H[-R_s L_{mm} i_{dsw} + \omega_r L_{ss} L_{mm} i_{qsw} + R_r L_{ss} i_{drw} + (\omega_s L_{mm}^2 - (\omega_s - \omega_r).L_{SS} L_{rr}) i_{qrw} - L_{ss} V_{drw} + L_{mm} V_{dsw}] \\ \dfrac{di_{qrw}}{dt} = H[-\omega_r L_{ss} L_{mm} i_{dsw} - R_s L_{mm} i_{qsw} + (-\omega_s L_{mm}^2 + (\omega_s - \omega_r).L_{SS} L_{rr}) i_{drw} + R_r L_{ss} i_{qrw} - L_{ss} V_{qrw} + L_{mm} V_{qsw}] \end{cases} \quad (26)$$

$$K = \begin{bmatrix} -0.6578 & 1.3214 & -7.2346 & 5.1104 & 0.5467 & 2.3791 & 4.3639 & -3.6218 & 0.6435 & 0.1654 & -0.5672 & 3.4562 & -2.4567 \\ -0.7891 & 1.0678 & 5.3211 & -0.9875 & -1.8976 & 1.7654 & -5.6784 & -4.4566 & 1.3211 & 0.8745 & 0.5678 & -1.4567 & -1.0678 \end{bmatrix}^T$$

$$L = \begin{bmatrix} -2.4501 & -1.5647 & -2.7716 & -1.6557 & -3.8121 & -2.3116 & -0.7891 & -2.3456 & -0.9876 & -1.1245 & -2.1456 & -1.5431 & -0.5671 \\ -1.9123 & -1.5671 & -2.0677 & -1.9544 & -2.7891 & -1.766 & -1.7654 & -0.5456 & -2.5671 & -2.5673 & -1.7893 & -3.456 & -1.0543 \end{bmatrix}^T$$

Credit Authorship Contribution Statement

Babak Keshavarz Zahed: Conceptualization, Data curation, Formal analysis, Funding acquisition, Investigation, Methodology, Resources, Software, Visualization, Writing - review & editing. **Mohammad Hossan Moradi**: Project administration, Supervision, Validation, Writing - original draft, Writing - review & editing.

Declaration Of Competing Interest

The authors declare that they have no known competing financial interests or personal relationships that could have appeared to influence the work reported in this paper. The ethical issues; including plagiarism, informed consent, misconduct, data fabrication and/or falsification, double publication and/or submission, redundancy has been completely observed by the authors.

References

[1] R. Arjmandzadeh, M. Banejad, and A. Akbarzadeh Kalat, "Improving the performance of a vsg in the distorted grid using third-order generalized integrator," *Journal of Applied Research in Electrical Engineering*, vol. 3, no. 1, pp. 1-8, 2024.

[2] M. Darabian, A. Bagheri, and S. Yousefi, "Design of a new robust controller for voltage regulation of DC link in wind-farm-side converter integrated with a hybrid AC and DC large-scale power system," *IET Generation, Transmission & Distribution*, vol. 17, no. 7, pp. 1674-1685, 2023.

[3] S. Aminzadeh, M. Tarafdar Hagh, and H. Seyedi, "Reactive power coordination between solid oxide fuel cell and battery for microgrid frequency control," *Journal of Applied Research in Electrical Engineering*, vol. 1, no. 3, pp. 121-130, 2022.

[4] M. Zolfaghari, G. B. Gharehpetian, and A. Anvari-Moghaddam, "Quasi-Luenberger observer-based robust DC link control of UIPC for flexible power exchange control in hybrid microgrids," *IEEE Systems Journal*, vol. 15, no. 2, pp. 2845-2854, 2020.

[5] J. Ma *et al.*, "A low frequency oscillation suppression method for grid-connected DFIG with virtual inertia," *International Journal of Electrical Power & Energy Systems*, vol. 144, p. 108531, 2023.

[6] M. Darabian, and A. Bagheri, "Stability improvement of large-scale power systems including offshore wind farms and MTDC grid aiming at compensation of time delay in sending robust damping signals," *International Journal of Electrical Power & Energy Systems*, vol. 143, p. 108491, 2022.

[7] L. Xiong *et al.*, "Optimal allocation of energy storage system in DFIG wind farms for frequency support considering wake effect," *IEEE Transactions on Power Systems*, vol. 37, no. 3, pp. 2097-2112, 2021.

[8] C. Olivieri *et al.*, "Application of an integrated RNN-ensemble method for the short-term forecast of inter-area oscillations modal parameters," E*lectric Power Systems Research*, vol. 225, p. 109790, 2023.

[9] S. Galvani, B. Mohammadi-Ivatloo, M. Nazari-Heris, and S. Rezaeian, "Optimal allocation of static synchronous series compensator (SSSC) in wind-integrated power system considering predictability," E*lectric Power Systems Research*, vol. 191, p. 106871, 2021.

[10] C. Maddela, and B. Subudhi, "Robust wide-area TCSC controller for damping enhancement of inter-area oscillations in an interconnected power system with actuator saturation," *International Journal of Electrical Power & Energy Systems*, vol. 105, pp. 478-487, 2019.

[11] A. Movahedi, A. H. Niasar, and G. Gharehpetian, "Designing SSSC, TCSC, and STATCOM controllers using AVURPSO, GSA, and GA for transient stability improvement of a multi-machine power system with PV and wind farms," *International Journal of Electrical Power & Energy Systems*, vol. 106, pp. 455-466, 2019.

[12] R. K. Singh, and N. K. Singh, "Power system transient stability improvement with FACTS controllers using SSSC-based controller," *Sustainable Energy Technologies and Assessments*, vol. 53, p. 102664, 2022.

[13] J. Im, J. Ban, Y. Kim, and J. Zhao "PMU-based distributed state estimation to enhance the numerical stability using equality constraints," *IEEE Transactions on Power Systems*, vol. 39, no. 2, pp. 4409 - 4421, 2023.

[14] Y. Yao, Y. Xu, M. Chow, "Distributed optimal dynamic communication paths planning for PMUs in the WAMS communication network," *IEEE Transactions on Industrial Informatics*, vol. 19, no. 9, pp. 9609-9618, 2023.

[15] M. Bhadu, N. Senroy, I. N. Kar, and G. N. Sudha, "Robust linear quadratic Gaussian-based discrete mode wide area power system damping controller," *IET Generation, Transmission & Distribution*, vol. 10, no. 6, pp. 1470-1478, 2016.

[16] H. Zhao, Z. Lin, Q. Wu, and S. Huang, "Model predictive control based coordinated control of multi-terminal HVDC for enhanced frequency oscillation damping," *International Journal of Electrical Power & Energy Systems*, vol. 123, p. 106328, 2020.

[17] D. Roberson, J. F. O'Brien, "Multivariable loop-shaping control design for stability augmentation and oscillation rejection in wide-area damping using HVDC," *Electric Power Systems Research*, vol. 157, pp. 238-250, 2018.

[18] M. Beiraghi, and A. M. Ranjbar, "Additive model decision tree-based adaptive wide-area damping controller design," *IEEE Systems Journal*, vol. 12, no. 1, pp. 328-339, 2016.

[19] ME. Bento, "Fixed low-order wide-area damping controller considering time delays and power system operation uncertainties," *IEEE Transactions on Power Systems*, vol. 35, no. 5, pp. 3918-3926, 2020.

[20] P. Gupta, A. Pal, and V. Vittal, "Coordinated wide-area damping control using deep neural networks and reinforcement learning," *IEEE Transactions on Power Systems*, vol. 37, no. 1, pp. 365-376, 2022.

[21] M. R. Paternina *et al.*, "Enhancing wide-area damping controllers via data-assisted power system linear models," *Electric Power Systems Research*, vol. 217, p. 109085, 2023.

[22] C. O. Maddela, and B. Subudhi, "Delay-dependent supplementary damping controller of tcsc for interconnected power system with time-delays and actuator saturation," *Electric Power Systems Research*, vol. 164, pp. 39-46, 2018.

[23] A. Sengupta, and D. K. Das, "Mitigating inter-area oscillation of an interconnected power system considering time-varying delay and actuator saturation," *Sustainable Energy, Grids and Networks*, vol. 27, pp. 100484, 2021.

[24] A. Paul, I. Kamwa, G. Joos, "Centralized dynamic state estimation using a federation of extended Kalman filters with intermittent PMU data from generator terminals," *IEEE Transactions on Power Systems*, vol. 33, no. 6, pp. 6109-6119, 2018.

[25] A. Paul, I. Kamwa, G. Joos, "PMU signals responses-based RAS for instability mitigation through on-the fly identification and shedding of the run-away generators," *IEEE Transactions on Power Systems*, vol. 35, no. 3, pp. 1707-1717, 2019.

[26] M. Bento, "A hybrid particle swarm optimization algorithm for the wide-area damping control design," *IEEE Transactions on Industrial Informatics*, vol. 18. no. 1, pp. 592-599, 2021.

[27] S. Mukherjee, A. Chakrabortty, H. Bai, A. Darvishi, and B. Fardanesh, "Scalable designs for reinforcement learning-based wide-area damping control," *IEEE Transactions on Smart Grid*, vol. 12. No. 3, pp. 2389-2401, 2021.

[28] Y. J. Isbeih, S. Ghosh, M. S. Moursi, and E. F. El-Saadany. "Online DMDc based model identification approach for transient stability enhancement using wide area measurements," *IEEE Transactions on Power Systems*, vol. 36, no. 5, pp. 4884-4887, 2021.

[29] W. Yao, et al, "Resilient wide-area damping control for inter-area oscillations to tolerate deception attacks," IEEE Transactions on Smart Grid, vol. 12, no. 5, pp. 4238-4249, 2021.

[30] W. Wu, X. Wang, H. Rao, B. Zhou, "Delay-dependent wide-area damping controller synthesis approach using Jensen's inequality and evolution algorithm," CSEE Journal of Power and Energy Systems, vol. 9, no. 5, pp. 1774-1785, 2022.

[31] F. Liu, R. Yokoyama, Y. Zhou, and M. Wu, "Free-weighting matrices-based robust wide-area FACTS control design with considering signal time delay for stability enhancement of power systems," *IEEJ Transactions on Electrical and Electronic Engineering*, vol. 7, no. 1, pp. 31-39, 2012.

[32] A. Prakash, K. Kumar, and S. Parida, "Energy capacitor system based wide-area damping controller for multiple inter-area modes," *IEEE Transactions on Industry Applications*, vol. 58, no. 2, pp. 1543-1553, 2022.

[33] T. N. Pham, A. M. Oo, and H. Trinh, "Event-triggered mechanism for multiple frequency services of electric vehicles in smart grids," *IEEE Transactions on Power Systems*, vol. 37, no. 2, pp. 967-981, 2021.

[34] C. W. Taylor, "BPA's wide-area stability and voltage control system (WACS) for blackout prevention," in *Proc. IEEE PES Power Systems Conference and Exposition*, vol. 3, p. 1610, 2004.

[35] E. Fridman, U. Shaked, "Delay-dependent stability and H∞ control: constant and time-varying delays," *International Journal of Control*, vol. 76, no. 1, pp. 48-60, 2010.

[36] H. Gao, J. Lam, C. Wang, and Y. Wang, "Delay-dependent output-feedback stabilisation of discrete-time systems with time-varying state delay," *IEE Proceedings-Control Theory and Applications*, vol. 151. no. 6, pp. 691-698, 2004.

[37] M. S. Sadabadi, and D. Peaucelle, "From static output feedback to structured robust static output feedback: A survey," *Annual Reviews in Control*, vol. 42, pp. 11-26, 2016.

[38] H. Shayeghi, and A. Ghasemi, "A multi objective vector evaluated improved honey bee mating optimization for optimal and robust design of power system stabilizers," *International Journal of Electrical Power & Energy Systems*, vol. 62, pp. 630-645, 2014.

[39] T. Surinkaew, and I. Ngamroo, "Adaptive signal selection of wide-area damping controllers under various operating conditions," *IEEE Transactions on Industrial Informatics*, vol. 14, no. 2, pp. 639-651, 2017.

[40] M. Darabian, and A. Jalilvand, "Predictive control strategy to improve stability of DFIG-based wind generation connected to a large-scale power system," *International Transactions on Electrical Energy Systems*, vol. 27, no. 5, pp. 2300, 2017.

[41] B. Lei, and S. Fei, " A brand new nonlinear robust control design of SSSC for transient stability and damping improvement of multi-machine power systems via pseudo-generalized Hamiltonian theory," *Control Engineering Practice*, vol. 29, pp. 147-157, 2014.

[42] A. Samosir, and A. Yatim, "Implementation of dynamic evolution control of bidirectional DC–DC converter for interfacing ultracapacitor energy storage to fuel-cell system," *IEEE Transactions on Industrial Electronics*, vol. 57, no. 10, pp. 3468-3473, 2010.

[43] V. Vittal, J. McCalley, P. Anderson, and A. Fouad, *Power system control and stability*. John Wiley & Sons, 2019.